INT. J. NUM. METH. HEAT FLUID FLOW, VOL. 2, 227–234 (1992)

NATURAL CONVECTION WITHIN A SIMPLIFIED MODEL OF THE HUMAN EYE

VIJAY K. GARG*

Department of Mechanical Engineering, University of Pittsburgh, Pittsburgh, PA 15261, USA

ABSTRACT

A finite difference solution for steady natural convective flow within the human eye, modelled as a sphere with a specified temperature distribution over its surface, has been obtained. The stream function–vorticity formulation of the equations of motion for the unsteady axisymmetric flow is used; interest lying in the final steady solution. Forward differences are used for the time derivatives and second-order central differences for the space derivatives. The alternating direction implicit method is used for solution of the discretization equations. Local one-dimensional grid adaptation is used to resolve the steep gradients in some regions of the flow at large Rayleigh numbers. The break-up into multi-cellular flow is found at high Rayleigh numbers. Results identify regions of stagnant fluid in locations similar to those of blind spots in the eye.

KEY WORDS Human eye Natural convection flow Temperature distribution

NOMENCLATURE

a_θ	false transient factor for temperature
a_Ψ	false transient factor for stream function
a_Ω	false transient factor for vorticity
g	acceleration due to gravity
Gr	Grashof number
Pr	Prandtl number of the fluid
r	radial coordinate measured from the centre of the sphere
r_e	radius of the eye (sphere)
R	dimensionless radial coordinate
Ra	Rayleigh number $= Gr\,Pr$
ΔR	mesh size in the radial direction
t	time
T	temperature of the fluid
T_1	maximum temperature of the eye surface
T_2	minimum temperature of the eye surface
u	velocity component in the ϕ direction
U	dimensionless velocity component in the ϕ direction
v	radial velocity component
V	dimensionless radial velocity component

Greek

α	thermal diffusivity of the fluid
β	coefficient of volumetric expansion of the fluid
$\Delta\phi$	mesh size in the ϕ direction
$\Delta\tau$	dimensionless time step
ϕ	latitude angle measured clockwise from the North position
ν	kinematic viscosity of the fluid
θ	dimensionless temperature
τ	dimensionless time
ω	dimensional vorticity
Ω	dimensionless vorticity
ψ	dimensional stream function
Ψ	dimensionless stream function

Subscripts

b	value at the boundary
$b+1$	value at one mesh length ΔR away from the boundary
s	refers to the eye surface
max	maximum value
min	minimum value

* Present address: NASA Lewis Research Center, Cleveland, Ohio 44135, USA.

0961–5539/92/030227–08$2.00

Received June 1991.
Revised January 1992

INTRODUCTION

Temperature variations within the human eye remain largely unstudied. A few reports in the literature deal with measurements of intraocular temperatures in animal eyes[1–4], but we are not aware of meaningful data available on human eyes. It is well established that the retina is one of the most metabolically active areas in the human body, and that the blood flow rate of the choriocapillaris, which provides nutrition to the retina, is extremely high. Retinal function is dependent upon biochemical reactions within the rods, cones, and retinal neural cells. It is reasonable to assume that variations in temperature could affect the rates of biochemical reactions within the retina. The possible effects of temperature changes within the eye include alteration of visual function, development of retinal degenerative diseases, role of drugs administered within the eye for certain infections or inflammations, etc. In addition to the atmospheric alteration of temperature, the use of intense illumination during examination of the eye and during surgical procedures on the globe can influence tissue temperature levels. There are cases where operating microscopes have been implicated in retinal burns during cataract surgery.

This analysis was therefore undertaken to study the effect of temperature changes on the flow patterns within the human eye in an effort to evaluate the role of temperature in the proper functioning of the eye. The eyeball is situated in the anterior part of the orbital cavity and is roughly spherical in shape. The anteriorly placed biconvex lens divides the eyeball cavity into two parts. The posterior part is filled with a jelly-like vitreous body, and the anterior with the fluid aqueous humor. Both fluids have properties very similar to those of water. It is known that the temperature of the retina is higher than that of the cornea due to latter's exposure to the atmosphere. The actual distribution of temperature along the eyeball surface is, however, unknown, and will be assumed for this study. Any other distribution can be easily handled. This temperature distribution causes natural convection currents within the fluid filled in the eye. The present study analyses this convection pattern with a view to determine regions of stagnant fluid that have clinical implications. The eye is modelled as a sphere containing water at 37°C, and subject to a specified temperature distribution over its surface.

While there are several studies available on the natural convective flow within a spherical annulus (see Gardner *et al.*[5] for a list of references), there are very few studies on the flow within a sphere. A transient solution in powers of Grashof number for water cooling in a sphere was first obtained by Pustovoit[6]. However, he carried the solution to only the first order, and thus presented results for $Gr=300$ and $Pr=6.75$ for a dimensionless time of unity. Whitley and Vachon[7] carried out a finite difference solution for transient convection in a sphere due to a sudden change of surface temperature. However, they could carry their solution to a small time only due to a slow numerical procedure. Chow and Akins[8] investigated experimentally the pseudo-steady natural convection of water in a sphere with a fixed difference between the surface and centre temperatures, and found differences between their results and those of Whitley and Vachon[7]. More recently, Mochimaru[9] used a Fourier series in latitude to solve for the transient convection within a sphere generated by a step change in wall temperature. This as well as the analysis of Shiina[10] is in Japanese. Shiina solved the integral boundary layer equations using fourth-order polynomials for the velocity and temperature profiles for the case when the sphere surface is cooled with a stagnation point at the top of the sphere.

From the above description, it is apparent that no study of the natural convective flow within a sphere subjected to a specified temperature distribution at its surface is available. We therefore describe a finite difference method that is fast, reliable and accurate for the steady axisymmetric natural convection heat transfer of a viscous fluid enclosed within a sphere. The equations of motion for the unsteady flow are solved to get the steady state solution. The method can also be applied to other geometries and boundary conditions.

ANALYSIS

As described above, the eye is modelled as a sphere filled with water, and having a specified temperature variation along the spherical wall. We can assume the flow within the sphere to be

axisymmetric, that is, independent of longitude, thereby analysing the flow within the half sphere only. Assuming constant properties except density, and using the Boussinesq approximation and spherical coordinates, the unsteady dimensionless energy and Navier–Stokes equations in the stream function–vorticity form are:

$$Pr\frac{\partial\theta}{\partial\tau}+Pr\,Gr^{1/2}\left(V\frac{\partial\theta}{\partial R}+\frac{U}{R}\frac{\partial\theta}{\partial\phi}\right)=\nabla^2\theta \tag{1}$$

$$D^2\Psi+R\Omega\sin\phi=0 \tag{2}$$

$$\frac{\partial\Omega}{\partial\tau}+Gr^{1/2}\left[V\frac{\partial\Omega}{\partial R}+\frac{U}{R}\frac{\partial\Omega}{\partial\phi}-\frac{\Omega}{R}(V+U\cot\phi)\right]$$
$$=-Gr^{1/2}\left(\sin\phi\frac{\partial\theta}{\partial R}+\frac{\cos\phi}{R}\frac{\partial\theta}{\partial\phi}\right)+\nabla^2\Omega-\frac{\Omega}{R^2\sin^2\phi} \tag{3}$$

where

$$\nabla^2=\frac{\partial^2}{\partial R^2}+\frac{2}{R}\frac{\partial}{\partial R}+\frac{1}{R^2}\frac{\partial^2}{\partial\phi^2}+\frac{\cot\phi}{R^2}\frac{\partial}{\partial\phi}$$

$$D^2=\frac{\partial^2}{\partial R^2}+\frac{1}{R^2}\frac{\partial^2}{\partial\phi^2}-\frac{\cot\phi}{R^2}\frac{\partial}{\partial\phi}$$

Here θ, Ψ and Ω are the dimensionless temperature, stream function and vorticity, respectively; R is the dimensionless radial coordinate; ϕ is the latitude angle measured clockwise from the vertically upward position; τ is the dimensionless time; V and U are the dimensionless velocity components in R and ϕ directions, respectively, and Gr and Pr are the Grashof and Prandtl numbers defined as:

$$\theta=\frac{T-T_2}{T_1-T_2}\qquad \Psi=Gr^{-1/2}\frac{\psi}{r_e\nu}\qquad \Omega=Gr^{-1/2}\frac{\omega r_e^2}{\nu}$$

$$\tau=\frac{t\nu}{r_e^2}\qquad R=\frac{r}{r_e}\qquad Gr=\frac{g\beta(T_1-T_2)r_e^3}{\nu^2}\qquad Pr=\frac{\nu}{\alpha}$$

$$V=Gr^{-1/2}\frac{vr_e}{\nu}=\frac{1}{R^2\sin\phi}\frac{\partial\Psi}{\partial\phi}\qquad U=Gr^{-1/2}\frac{ur_e}{\nu}=-\frac{1}{R\sin\phi}\frac{\partial\Psi}{\partial R}$$

This scaling is suggested in the literature[11,12] for Pr of order unity and large Gr. Also, following de Vahl Davis[12], the energy equation (1) has been multiplied by Pr so that the solution time is almost independent of the Prandtl number. Here, T, ψ, ω, v, u, and t are the dimensional counterparts of θ, Ψ, Ω, V, U and τ, respectively, and r is the radial coordinate. Also, T_1 and T_2 are the maximum and minimum temperatures, respectively, of the eye surface, ν and α are the kinematic viscosity and thermal diffusivity of the fluid, respectively, g is the acceleration due to gravity, and β is the coefficient of thermal expansion.

Due to axisymmetry (solution independent of the longitude), only half the domain need be considered. The following boundary and initial conditions apply:

$$\partial\Psi/\partial R=0\qquad \partial\theta/\partial R=0\qquad \partial\Omega/\partial R=0\qquad \text{at}\quad R=0$$

$$\Psi=0\qquad \theta=\theta_s(\phi)\qquad \Omega=-\frac{1}{\sin\phi}\frac{\partial^2\Psi}{\partial R^2}\qquad \text{at}\quad R=1 \tag{4}$$

$$\Psi=0\qquad \partial\theta/\partial\phi=0\qquad \Omega=0\qquad \text{at}\quad \phi=0,\pi$$

$$\Psi=0\qquad \theta=0\qquad \Omega=0\qquad \text{at}\quad \tau=0$$

Here $\theta_s(\phi)$ represents the dimensionless temperature variation over the eye surface. It has not yet been measured for the human eye. For this analysis, it is assumed to be sinusoidal, varying from 0 (temperature T_2) at the top to 1 (temperature T_1) at the bottom of the sphere. This yields $\theta_s(\phi)$ varying from 0 to 1/2 for $0 \leqslant \phi \leqslant 60°$, and from 1/2 to 1 for $60° \leqslant \phi \leqslant 180°$. It is, thus, in conformity with the fact that a larger temperature variation occurs near the cornea (exposed to the ambient) than that over the retinal wall. It is known that $T_1 - T_2 \approx 3.3°C$. Any other variation of $\theta_s(\phi)$ can be easily incorporated.

NUMERICAL TECHNIQUE

Following de Vahl Davis[12], we introduce the false transient equations in order to reduce the computer time required for a numerical solution of (1)–(4). The changes to the equations are the introduction of false transient factors a_θ, a_Ω and a_Ψ and the addition of a transient term to (2) to turn it into a parabolic equation. Thus (1)–(3) are written as:

$$\frac{Pr}{a_\theta}\frac{\partial\theta}{\partial\tau} + Pr\,Gr^{1/2}\left(V\frac{\partial\theta}{\partial R} + \frac{U}{R}\frac{\partial\theta}{\partial\phi}\right) = \nabla^2\theta \tag{5}$$

$$\frac{1}{a_\Psi}\frac{\partial\Psi}{\partial\tau} = D^2\Psi + R\Omega\sin\phi \tag{6}$$

$$\frac{1}{a_\Omega}\frac{\partial\Omega}{\partial\tau} + Gr^{1/2}\left[V\frac{\partial\Omega}{\partial R} + \frac{U}{R}\frac{\partial\Omega}{\partial\phi} - \frac{\Omega}{R}(V + U\cot\phi)\right] = -Gr^{1/2}\left(\sin\phi\frac{\partial\theta}{\partial R} + \frac{\cos\phi}{R}\frac{\partial\theta}{\partial\phi}\right) + \nabla^2\Omega - \frac{\Omega}{R^2\sin^2\phi} \tag{7}$$

The false transient factors change the time scales of the governing equations, leading to a loss of the true transient solution, but the final steady state solution, if one exists, is unaffected. Optimum values of these factors, if found, speed up the convergence. Generally, numerical instability arises first in the vorticity equation (7) and a reduction in a_Ω, accompanied by a corresponding increase in a_θ and a_Ψ, permits solution to be obtained for larger parameter values[12]. No attempt was made to optimize the values of false transient factors.

For the finite difference solution of (5), (6), (7) and (4), forward differences are used for the time derivatives and second-order central differences for the space derivatives. The resulting algebraic equations are solved by the alternating direction implicit method, thus solving a set of tridiagonal equations every time. In accordance with de Vahl Davis[12], we found that the cell Reynolds number restriction resulting from the use of second-order central differences for convection terms is not overwhelming due to relatively small velocities in natural convection even at large Grashof numbers. In order to keep the solution numerically stable, the time step $\Delta\tau$ is limited to a value of the order of the square of the smaller of the two mesh sizes ΔR and $\Delta\phi$, with the false transient factors set to unity. In addition to their role in speeding up the convergence, these factors are used to postpone the numerical instability at sufficiently large values of the Grashof number.

It is well known that as the Grashof number increases, the boundary layer on the spherical wall gets thinner and there are large gradients in the ϕ direction as well. In order to resolve these radial and azimuthal gradients, it is necessary to have a high density of grid points near regions of large gradients. If the grid size is kept uniform, a very large number of grid points would result leading to a solution of a large set of equations. This would require excessive computer time and involve large round-off error. A practical solution is to use a fine mesh size near regions of large gradients, and larger mesh size elsewhere. In order to have a guided, rather than an arbitrary, uneven distribution of grid points, local one-dimensional grid adaptation, following Nakahashi and Deiwert's method[13], is used. It may be pointed out that a two-dimensional grid adaptation renders the grid non-orthogonal, thus requiring the solution

of a complex set of transformed equations owing to the presence of pseudo-diffusive terms. On the other hand, one-dimensional grid adaptation in each direction keeps the grid orthogonal, and, therefore, (5), (6), (7) and (4) remain unchanged. However, with an uneven distribution of grid points, the second-order central differences for space derivatives need to be modified, as described by Hornbeck[14].

The number of grid points were taken to be 41 in the radial direction and 46 in the ϕ direction at low Rayleigh numbers, and increased to 81 and 91, respectively, at high Ra. For $Ra < 10^4$, results with a 41×46 grid matched very well with those obtained with a 61×61 grid; maximum difference being less than 2%. The final solution of (5), (6), (7) and (4) is fed into a very similar code for steady state equations of motion (without the initial conditions and $\partial/\partial\tau$ terms) to ensure that the solution presented here is the steady state one. Hardly any iteration was required in this final step.

While the discretization of boundary conditions for Ψ and θ is straight forward, the boundary condition for Ω at $R=1$ is discretized, following Woods[15], as:

$$\Omega_b = \frac{-3\Psi_{b+1}}{(\Delta R_b)^2 \sin\phi_b} - \frac{R_{b+1}}{2}\Omega_{b+1}$$

where the subscripts 'b' and '$b+1$' denote values at a mesh point on the boundary and one mesh length ΔR away from the boundary, respectively. This is a second-order relation, thus matching with the discretization of the governing equations.

ACCURACY

Since no study, experimental or numerical, is available for convection within the eye or within a sphere with a variable temperature on its surface, a check on the solution was provided by solving the well-studied natural convection problem within a spherical annulus with isothermal walls, inner sphere being hotter than the outer. The governing differential equations for this case are the same; only some boundary conditions are different. A comparison was made for $Ra = 14{,}000$, $Pr = 0.7$ and diameter ratio of 2 with the results provided by Singh and Chen[16]. The results matched very well. There was excellent agreement between the isotherms and streamlines within the annulus, and between the local Nusselt numbers on the inner and outer spheres. The maximum value of the dimensionless stream function in our case is 0.2071 while theirs is 0.2076, and the location of this maximum coincides exactly. Moreover, while our average Nusselt number is 2.1331, Singh and Chen[16] found a value of 2.1439. Our results for this case are shown in *Figure 1* in terms of isotherms and streamlines. The isotherms in this and later

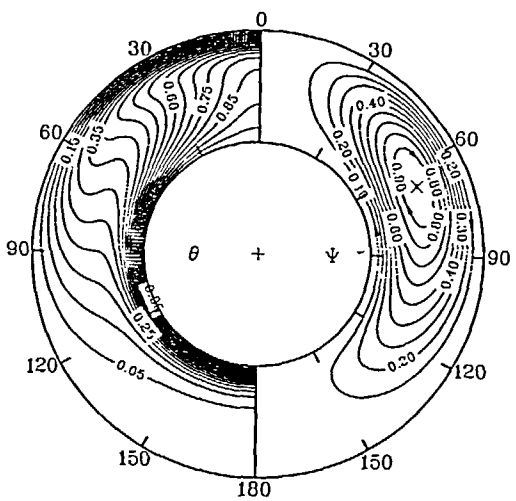

Figure 1 Isotherms and streamlines in a spherical annulus of diameter ratio 2 for $Ra = 14{,}000$, $Pr = 0.7$. $\Psi_{max} = 0.2071$

Figures have been drawn at intervals of 0.05, while the streamlines have been drawn at intervals of $\Psi_{max}/10$, with values of Ψ/Ψ_{max} displayed on the streamlines. The sign $\times$ indicates the location of Ψ_{max}, also known as the centre of rotation for the fluid in the half annulus. Singh and Chen[16] developed a series solution in terms of Legendre polynomials and Gegenbauer functions, but were unable to get accurate results for higher Rayleigh numbers due to premature truncation of the series solution[17]. Another check was provided by the fact that Nusselt number averaged over each of the spheres in the annulus was the same, and matched very well with values available in the literature. Owing to lack of data available in the literature on vorticity, no comparison could be made for its values.

RESULTS

All the results presented here are for a $Pr=4.63$ (water at 37°C). The mean eyeball diameter is about 23 mm, and the temperature difference, (T_1-T_2), is about 3.3°C. *Figure 2* shows the isotherms and streamlines for $Ra=11{,}275$ which corresponds to $(T_1-T_2)\approx 0.4$°C for the human eye. In this and later Figures, values of Ψ/Ψ_{max} are displayed on the streamlines. As shown by the streamlines, the flow is essentially anti-clockwise about the centre of rotation at $\phi\approx 110°$. The isotherms are crowded into the top of the cavity with a relatively large region around $\phi=90°$ being almost isothermal. As the Rayleigh number increases, implying an increase in (T_1-T_2), the single cell in *Figure 2* breaks-up into several cells. *Figure 3* shows the isotherms for $Ra=22{,}550$, twice that for *Figure 2*, and we notice a clockwise cell near the eyeball surface around $\phi=60°$. This cell is much weaker than the main eddy which is anti-clockwise. The isotherms have crowded more into the upper part of the cavity, increasing the temperature gradients for $\phi\leqslant 30°$.

As the Rayleigh number increases to 64,940, corresponding to $(T_1-T_2)\approx 2.4$°C, the clockwise cell, with a centre of rotation around $\phi=60°$, expands and gets stronger, as shown in *Figure 4*. The anti-clockwise main eddy has a centre of rotation at $\phi\approx 135°$. A large part of the cavity is almost isothermal, as shown by the isotherms. Finally, *Figure 5* shows the isotherms and streamlines for $Ra=89{,}310$ corresponding to $(T_1-T_2)\approx 3.3$°C, the condition pertaining to the human eye. At this Ra, there are four cells present, two anti-clockwise and two clockwise. The two newly formed cells are very weak compared to the already existing cells. Comparison of

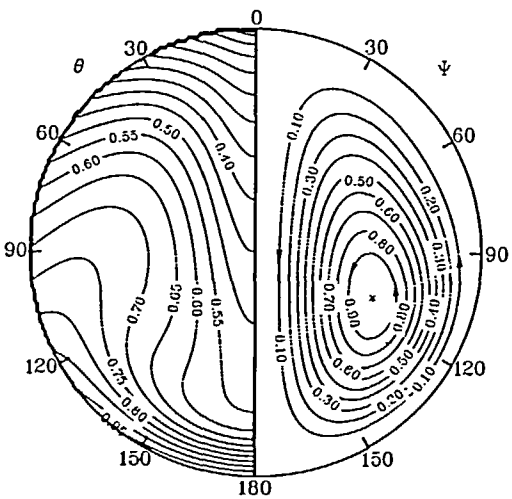

Figure 2 Isotherms and streamlines for $Ra=11{,}275$, $\Psi_{min}=-0.0143$

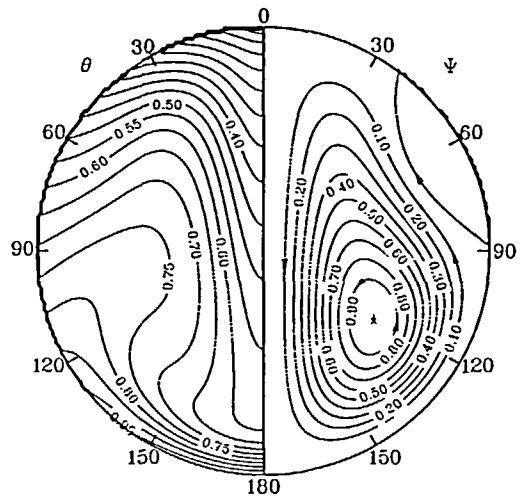

Figure 3 Isotherms and streamlines for $Ra=22{,}550$. $\Psi_{min}=-0.0126$

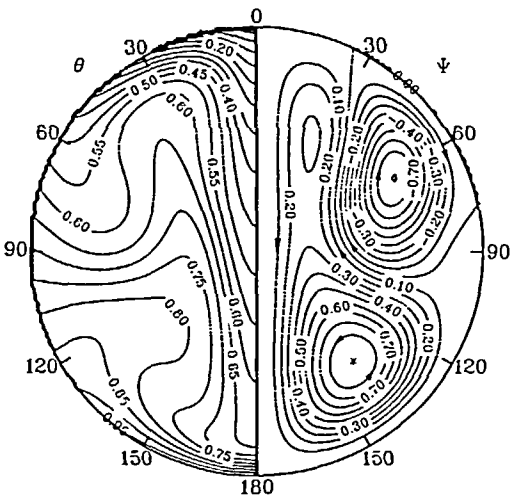

Figure 4 Isotherms and streamlines for $Ra=64{,}940$. $\Psi_{min}=-0.0076$

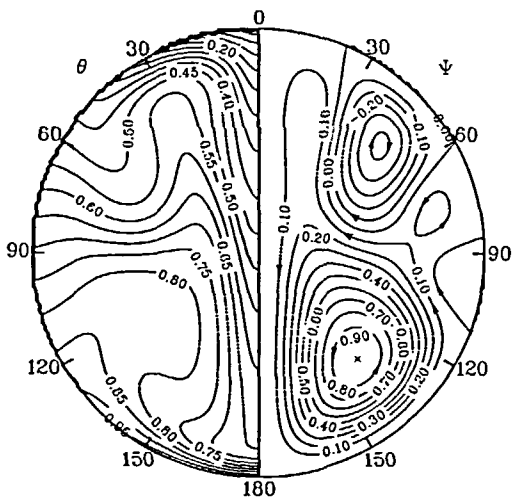

Figure 5 Isotherms and streamlines for $Ra=89{,}310$, $\Psi_{min}=-0.0084$

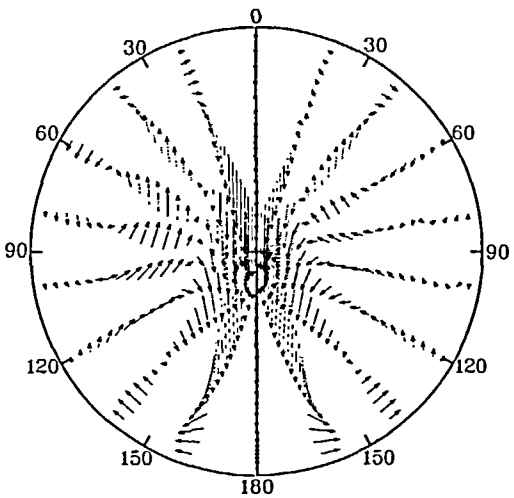

Figure 6 Velocity vectors for $Ra=89{,}310$ (right half; max. speed $=0.316$) and $Ra=40{,}590$ (left half; max. speed $=0.259$)

Figures 4 and *5* shows that the clockwise eddy with the centre of rotation around $\phi=60°$ is stronger in *Figure 4* (lower Rayleigh number) than that in *Figure 5* (higher Rayleigh number), while the anti-clockwise eddy with the centre of rotation around $\phi=135°$ is stronger at the higher Rayleigh number. Thus, it appears that the former (clockwise) eddy breaks up further into smaller eddies as Ra increases from 64,940 in *Figure 4* to 89,310 in *Figure 5*. The isotherms show a still larger region under nearly isothermal conditions.

Figure 6 shows the velocity vectors in the spherical cavity at two Rayleigh numbers. The velocity vectors, normalized by the maximum speed in the cavity for each Ra, have been drawn to scale in *Figure 6*, and represent the normalized velocity at the mid-point of the vector. These vectors are drawn at 20 equidistant radial positions and at 20° intervals in ϕ within the spherical

cavity. It may be noted that the maximum speed of flow is near the centre of the eye, and is only 2.6 mm/sec when $Ra=89{,}310$ and about 2.1 mm/sec when $Ra=40{,}590$ corresponding to $(T_1-T_2)\approx 1.5°C$. It is clear from *Figure 6* that the flow fields near $\phi=90°$ are quite different for the two Rayleigh numbers. For the higher Rayleigh number pertaining to the actual condition within the eye, velocity of the fluid around $\phi\approx 90°$ is very small for $R\approx 0.75$. Thus, there is an almost stagnant fluid in this region, and it is in this region that blind spots are found within certain eyes[18]. Apparently, the jelly-like vitreous body in the posterior part of the eye coagulates into an opaque body within the stagnant region due to lack of circulation, leading to the formation of blind spots. Owing to the lack of better data, these results are based on the assumption of a sinusoidal variation of temperature on the eyeball surface. While the flow field within the eye depends upon the surface temperature distribution, the finding that stagnation region within the eye is located where blind spots with certain eyes are found leads one to speculate that the actual temperature distribution on the eye surface may be close to the sinusoidal one.

CONCLUSIONS

An efficient numerical technique for the study of natural convection flow within the human eye, modelled as a sphere with a prescribed temperature variation over its surface, has been described. Results are presented for Prandtl number of 4.63 corresponding to water at 37°C. The break-up into multi-cellular flow is found at high Rayleigh numbers. Results identify regions of stagnant fluid in locations similar to those of blind spots in the eye.

ACKNOWLEDGEMENTS

Support from the Pittsburgh Supercomputing Center for use of its CRAY Y-MP/832 is gratefully acknowledged. The author is also grateful to Dr Thomas Friberg of the Eye and Ear Institute of Pittsburgh for introducing him to the problem and for useful discussions.

REFERENCES

1 Schwartz, B. and Feller, M. R. Temperature gradients in the rabbit eye, *Investig. Ophthalmol.*, **1**, 513–521 (1962)
2 Rosenbluth, R. F. and Fatt, I. Temperature measurements in the eye, *Exp. Eye Res.*, **25**, 325–341 (1977)
3 Parver, L. M., Auker, C. and Carpenter, D. O. Choroidal blood flow as a heat dissipating mechanism in the macula, *Am. J. Ophthalmol.*, **89**, 641–645 (1980)
4 Auker, C. R., Parver, L. M., Doyle, T. and Carpenter, D. O. Choroidal blood flow I. Ocular tissue temperature as a measure of flow, *Arch. Ophthalmol.*, **100**, 1323–1326 (1982)
5 Gardner, D. R., Douglass, R. W. and Trogdon, S. A. Linear stability of natural convection in spherical annuli, *J. Fluid Mech.*, **221**, 105–129 (1990)
6 Pustovoit, S. P. Transient thermal convection in a spherical cavity, *J. Appl. Math. Mech.*, **22**, 800–806 (1958)
7 Whitley, III H. G. and Vachon, R. I. Transient laminar free convection in closed spherical containers, *J. Heat Transfer*, **94**, 360–366 (1972)
8 Chow, M. Y. and Akins, R. G. Pseudosteady-state natural convection inside spheres, *J. Heat Transfer*, **97**, 54–59 (1975)
9 Mochimaru, Y. Transient natural convection heat transfer in a spherical cavity, *Nippon Gakkai Ronbunshu*, **53**(494), 3070–3075 (1987)
10 Shiina, Y. An analysis of heat transfer from the inner surface of a sphere by free convection (comparison with the experiment in a hemisphere), *Nippon Gakkai Ronbunshu*, **53**(496), 3742–3747 (1987)
11 Ostrach, S. Natural convection in enclosures, *J. Heat Transfer*, **110**, 1175–1190 (1988)
12 de Vahl Davis, G. Finite difference methods for natural and mixed convection in enclosures, *Proc. 8th Int. Heat Transfer Conf., San Francisco*, **1**, 101–109 (1986)
13 Nakahashi, K. and Deiwert, G. S. Self-adaptive-grid method with application to airfoil flow, *AIAA J.*, **25**, 513–520 (1987)
14 Hornbeck, R. W. Numerical marching techniques in fluid flows with heat transfer, *NASA SP-297* (1973)
15 Woods, L. C. A note on the numerical solution of fourth order differential equations, *Aero. Q.*, **5**, 176–184 (1954)
16 Singh, S. N. and Chen, J. Numerical solution for free convection between concentric spheres at moderate Grashof numbers, *Num. Heat Transfer*, **3**, 441–459 (1980)
17 Garg, V. K. Natural convection between concentric spheres, *Int. J. Heat Mass Transfer* (in press)
18 Friberg, T. R. personal communication